Long-eccentricity pacing of alluvial stratigraphic architecture in the Eocene Bighorn Basin, Wyoming, USA

Wang, Youwei; Baars, Timothy F.; Storms, Joep E.A.; Martinius, Allard W.; Gingerich, Philip D.; Abels, Hemmo A.

Important note
To cite this publication, please use the final published version (if applicable).
Please check the document version above.

Long-eccentricity pacing of alluvial stratigraphic architecture in the Eocene Bighorn Basin, Wyoming, USA

Youwei Wang[1,2], Timothy F. Baars[1], Joep E.A. Storms[1], Allard W. Martinius[1,3], Philip D. Gingerich[4], and Hemmo A. Abels[1,*]

[1]Department of Geosciences and Engineering, Delft University of Technology, Stevinweg 1, 2628 CN Delft, Netherlands
[2]Department of Environmental Sciences, University of Virginia, Charlottesville, Virginia 22904, USA
[3]Equinor ASA, Arkitekt Ebbellsvei 10, N–7053 Trondheim, Norway
[4]Museum of Paleontology, University of Michigan, Ann Arbor, Michigan 48109-1079, USA

ABSTRACT

Alluvial stratigraphy builds up over geologic time under the complex interplay of external climatic and tectonic forces and internal stochastic processes. This complexity makes it challenging to attribute alluvial stratigraphic changes to specific factors. Geological records indicate pronounced and persistent climatic changes during the Phanerozoic, while the effects of these changes on alluvial stratigraphy remain insufficiently documented. We provide evidence for 405 k.y. long-eccentricity climate forcing of alluvial stratigraphy in the lower Eocene Willwood Formation of the Bighorn Basin, Wyoming (USA). Two ∼90-m-thick intervals, characterized by a relative paucity of sand, dominance of sinuous-river channels, and floodplain sediments with better-developed paleosols, coincide with eccentricity maxima as determined through integrated stratigraphic methods. These intervals are interspersed with three contrasting intervals, marked by relatively high sand content, prevalent braided-river channels, and less-developed paleosols, corresponding to eccentricity minima. A comprehensive genetic model that integrates climate, source-to-sink system, and alluvial dynamics to explain these findings remains to be elucidated. Given the consistent presence of the 405 k.y. eccentricity cycle throughout Earth's history, it is plausible to infer that its influence may be discernible across a wide array of alluvial stratigraphic records.

INTRODUCTION

Alluvial stratigraphy serves as a tangible archive of Earth's history, shaped by dynamic and complicated processes (Hajek and Straub, 2017). These processes encompass both internal river dynamics, such as channel migration and avulsion, and external environmental influences, including climate, tectonics, and eustasy (Blum and Törnqvist, 2000). Distinguishing between changes in alluvial stratigraphy caused by inherent river behaviors and external forces is challenging due to their intertwined impacts. This complexity is amplified by the temporal and spatial variability of river systems, which may respond differently to similar external factors (Vandenberghe, 2001).

River styles reflect the quasi-equilibrium form of channels in response to water dis-

Youwei Wang https://orcid.org/0000-0003-1583-8415
*h.a.abels@tudelft.nl

charge, sediment flux, and slope (Lyster et al., 2022). The spectrum of river styles is broad, encompassing straight, sinuous, braided, and anastomosing rivers as end members, along with numerous intermediate forms (Church, 2006). Among these, braided and sinuous rivers are prevalent in current fluvial landscapes and alluvial stratigraphic records. These river styles are not mutually exclusive and can coexist within the same geographical region (Vandenberghe, 2001). Transitions between the styles can occur in response to climatic changes (Gibling, 2006; Foreman et al., 2012), such as the transition from sinuous to braided rivers during the Permian–Triassic mass extinction (e.g., Ward et al., 2000), and the frequent river style changes in response to Holocene glacial-interglacial cycles (Huisink, 2000).

Earth's orbital cycles significantly influence climate, leaving their imprint on alluvial records (Fielding and Webb, 1996; Westerhold et al., 2020; Opluštil et al., 2022). The 405 k.y.

eccentricity cycle has been correlated with significant fluvial changes, including alternations in fluvial progradation and retrogradation (Olsen and Kent, 1996; Smith et al., 2014), incision and aggradation (Vandenberghe, 2003; Noorbergen et al., 2020), and high and low amalgamation (Sharma et al., 2023). Despite these advances, the extent of astronomical climate control on alluvial stratigraphy remains under-explored and possibly under-appreciated.

We characterize the alluvial architecture of a 300-m-thick stratigraphic succession of excellent exposures of the lower Eocene Willwood Formation in the northern Bighorn Basin, Wyoming (United States). We built a composite stratigraphic framework based on floodplain aggradation cycles defined by Wang et al. (2023), which we dated by integrated stratigraphic data and compared to an astronomical target curve. The analysis shows and helps to explain variations in river styles and associated floodplain sediments. Lastly, we contextualize these changes in alluvial architecture within the broader scope of extrinsic climate forcing, intrinsic dynamics, and their interactions.

OUTCROP DATA SET AND METHODS
Study Area and Succession

We studied the Eocene Willwood Formation in the Deer Creek area of the McCullough Peaks in the northern Bighorn Basin, Wyoming (Fig. 1). The Bighorn Basin is a Laramide intermontane basin, with predominant northward drainage during the early Eocene (Owen et al., 2017; Wang et al., 2022) (Fig. 1). It has been reconstructed as a warm-temperate to subtropical environment with seasonal precipitation on a landscape resembling modern-day savannahs, where broad open areas are interspersed with forest-bordered streams (van Houten, 1944).
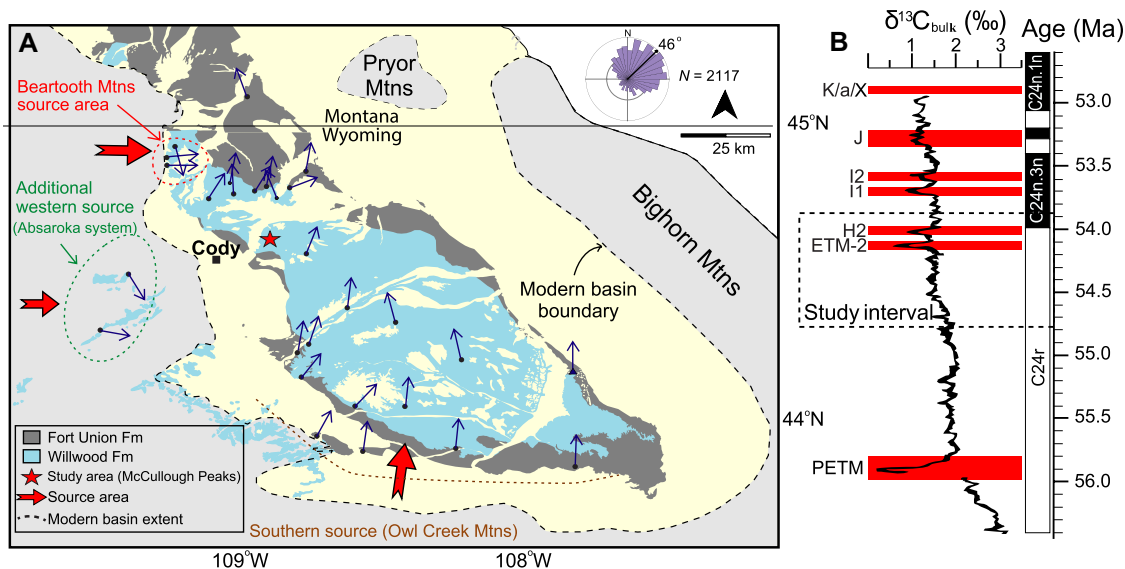
Figure 1. (A) Geographic location of the study area, McCullough Peaks, and the provenances of the Bighorn Basin, Wyoming, USA. Paleocurrent data are from Owen et al. (2017). Fm—Formation; Mtns—Mountains. (B) $\delta^{13}C_{bulk}$ data from Zachos et al. (2010). ETM—Eocene Thermal Maximum; PETM—Paleocene-Eocene Thermal Maximum. H, I, J, K, and X are warming events. C24n.1n, C24n.3n, and C24r are magnetic polarity chrons.

Floodplain Deposit Characterization and Stratigraphic Framework

We determined color reflectance (a*) by measuring matrix color in freshly broken rocks at 10 cm vertical resolution from four sections: Deer Creek Amphitheater (DCA) (Abels et al., 2013), Purple Butte (PB), Upper Deer Creek (UDC), and Creek Star Hill (CSH) (Fig. 2A). A measure for the degree of soil development was developed by Abels et al. (2013) for these series, correlating soil B (subsoil) horizon redness with pedogenesis intensity and identifying a* > 7 as indicative of significant pedogenesis. We used this threshold to identify well-developed paleosols.

A composite two-dimensional stratigraphic section was created using floodplain aggradation cycles identified by Wang et al. (2023). These cycles feature alternations between two distinct units: (1) overbank deposits with substantial pedogenic influence; and (2) avulsion belt deposits that lack extensive pedogenic influence (Abels et al., 2013) (Fig. 2B). These cycles are postulated to have formed during alternating phases of channel stability and instability (Abels et al., 2013; Wang et al., 2021) resulting from precession-scale climate change.

Sandstone Bodies and Their Stratigraphic Locations

Sandstone bodies were documented by Wang et al. (2022), including both field descriptions (n = 66; Fig. 2A) and photogrammetric images (n = 19). For simplicity, each sandstone body was interpreted as one of two end-member river styles: braided and sinuous rivers (Fig. 2C). Sandstone bodies showing extensive channel features (e.g., crossbedding, lateral accretion surfaces) were mapped in the photogrammetric model. Sandstone body width data were corrected for their inclination relative to

the average flow direction of 3° east of north (Wang et al., 2022).

Sandstone bodies were stratigraphically positioned by correlating them with the nearest laterally adjacent paleosol layer that is tied into the floodplain stratigraphic framework. When the intersection of a channel sandstone with a paleosol layer was not evident, its elevation was projected using data from the photogrammetric model.

Age Control

Age control is achieved by integrated constraints from biostratigraphy, magnetostratigraphy, and stable carbon isotope stratigraphy, which demonstrates the quasi-stable sedimentation rates in the northern Bighorn Basin on 100 k.y. time scales (Abels et al., 2012, 2016). The $\delta^{13}C$ record in pedogenic carbonate (Abels et al., 2012, 2016; Fig. 3C) has been correlated with the deep marine record at Ocean Drilling Program Site 1262 (Walvis Ridge, southern Atlantic Ocean; Zachos et al., 2010; Fig. 3B), revealing a high similarity that indicates both records accurately capture the carbon isotope signature of the global ocean–atmosphere reservoir (Abels et al., 2012). This correlation allows for importing the marine age model into the Bighorn alluvial stratigraphy, further enabling correlation to the normalized eccentricity curve constructed by Zeebe and Lourens (2019) (Fig. 3A).

RESULTS

There are two types of stratigraphic intervals: one characterized by predominantly (>60%) sinuous river styles and redder floodplain sediments (i.e., the proportion of a* > 7 is higher than 20%); the other featuring predominantly braided river styles coupled with less-red sediment (i.e., the proportion of a* > 7 is less than 20%).

Interval I has a limited distribution in the photogrammetric model, and it includes three floodplain aggradation cycles (cycles A to C; Fig. 3E), totaling 18 m. Of three sandstone bodies, two are interpreted as braided (Fig. 3), based on characteristics of sandstone bodies and less-red sediment (i.e., the proportion of a* > 7 is 16%).

Interval II encompasses 12 floodplain aggradation cycles (cycles D–O; Fig. 3E), totaling 87 m. It includes 22 sinuous and 14 braided channel sandstone bodies, with average dimensions of 299 m × 9.0 m and 165 m × 6.2 m, respectively (Fig. S2 in the Supplemental Material[1]). Intensely red intervals (a* > 7) constitute 22% of the total thickness (Fig. 4B).

Interval III includes 11 floodplain aggradation cycles (cycles Q–Z), totaling 73 m. It features 24 braided and 4 sinuous channel sandstone bodies, with average dimensions of 204 m × 6.2 m and 106 m × 9.0 m, respectively (Fig. S2). Floodplain deposits are overall less red, with intensely red intervals constituting 17% of the total thickness (Fig. 4).

Interval IV (cycles P1–P13), totaling 90 m and with Eocene Thermal Maximum 2 (ETM2) and H2 hyperthermals (Abels et al., 2016), displays a balanced distribution of river styles (10 sinuous, 8 braided) but leans toward sinuous dominance compared to Interval III. Intensely red intervals (a* > 7) constitute 27% of the total thickness, similar to Interval II.

Interval V, stratigraphically above Interval IV, lacks quantitative data in the current study. Qualitative observations in the field and pho-

---

[1]Supplemental Material. Figure S1 (UAV-based photogrammetric model in the LIME software) and Figure S2 (comparison of channelized sandstone width and depth in Intervals II and III exhibiting varying dominance of river styles). Please visit https://doi.org/10.1130/GEOL.S.25683864 to access the supplemental material; contact editing@geosociety.org with any questions.
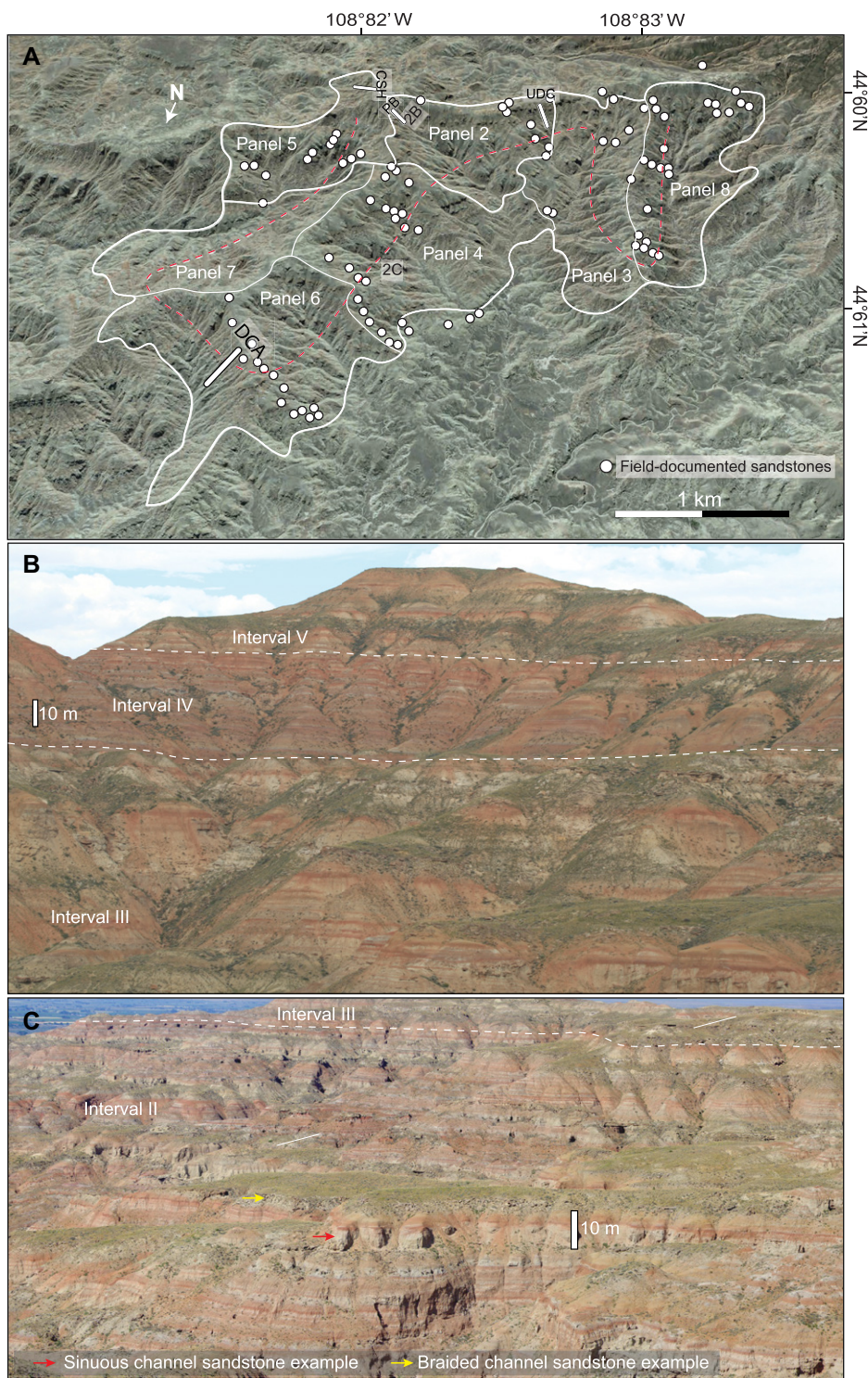
Figure 2. Unmanned aerial vehicle–based photogrammetric model and field photographs of the study area in the Bighorn Basin, Wyoming, USA (see Fig. 1). (A) Locations of field-documented sandstones in photogrammetric panels. The red dashed line indicates how the composite section of Figure 3F was constructed. Trenched sections (white bars) include Deer Creek Amphitheater (DCA), Purple Butte (PB), Upper Deer Creek (UDC), and Creek Star Hill (CSH). (B) Field photograph showing the floodplain-rich nature of the studied stratigraphy. (C) Field photograph comparing sinuous and braided channel deposits viewed from a distance. Locations of panels B and C are approximated in panel A.

tope excursions as tie points (Figs. 3B and 3C). Eccentricity maxima were separated from minima by the mean normalized eccentricity. The correlation suggests that Intervals II and IV correspond closely to eccentricity maxima, while Intervals I, III, and V coincide with eccentricity minima.

DISCUSSION AND CONCLUSIONS
Long-Eccentricity Control on Alluvial Architecture

Long-eccentricity minima align with dominant braided channels, less-developed paleosols, and higher sand content, while long-eccentricity maxima are associated with prevalent sinuous channels, more-developed paleosols, and lower sand content. Classifying river styles introduces an element of subjectivity (Fielding et al., 2018; Lyster et al., 2022), and some of the identified river styles may represent transitional states between sinuous and braided categories (Church, 2006). This could be complicated by the coexistence of sinuous and braided river styles in both present-day landscapes and the geologic record (Vandenberghe, 2001). Therefore, our approach attributing sandstone bodies to one or the other of two formative river styles may be simplistic. Nonetheless, the predominance of one river style over the other within each interval provides a compelling link between astronomical climate forcing and alluvial stratigraphy.

This temporal overlap complicates the direct interpretation of the impact of eccentricity on alluvial stratigraphy in Interval IV, as part of the observed changes may be attributable to the hyperthermal events occurring in that interval. The Paleocene–Eocene Thermal Maximum (PETM), having a magnitude twice that of the ETM2 (Abels et al., 2012), is linked with expansion and coarsening of alluvial facies (Foreman et al., 2012; Pujalte et al., 2015), a shift to more red-purple soil hues, and overall stronger pedogenesis in the Bighorn Basin (Kraus et al., 2015). The PETM is characterized by increased runoff variability, leading to a predominance of braided-river patterns in the Bighorn Basin (Foreman, 2014). A similar, although less pronounced, effect on river styles is likely to occur during ETM2 and H2 events, potentially resulting in a greater prevalence of braided over sinuous river styles in Interval IV, as compared to the preceding eccentricity maximum in Interval II. However, the specific impact of ETM2 on alluvial systems remains insufficiently understood (Abels et al., 2012), leaving this hypothesis open for further investigation.

Environmental Interpretation of Observed Alluvial Stratigraphic Changes

On the Willwood Formation floodplains, a higher degree of soil B redness has been interpreted to indicate stronger pedogenesis (Abels et al., 2013), which could be driven

togrammetric models suggest that Interval V resembles Interval III, where braided river styles and less-red floodplain deposits are predominant (Fig. 2B).

As described above, the stratigraphic section of the Bighorn Basin (Fig. 3F) was correlated with the normalized eccentricity curve (Zeebe and Lourens, 2019; Fig. 3A) using carbon iso-
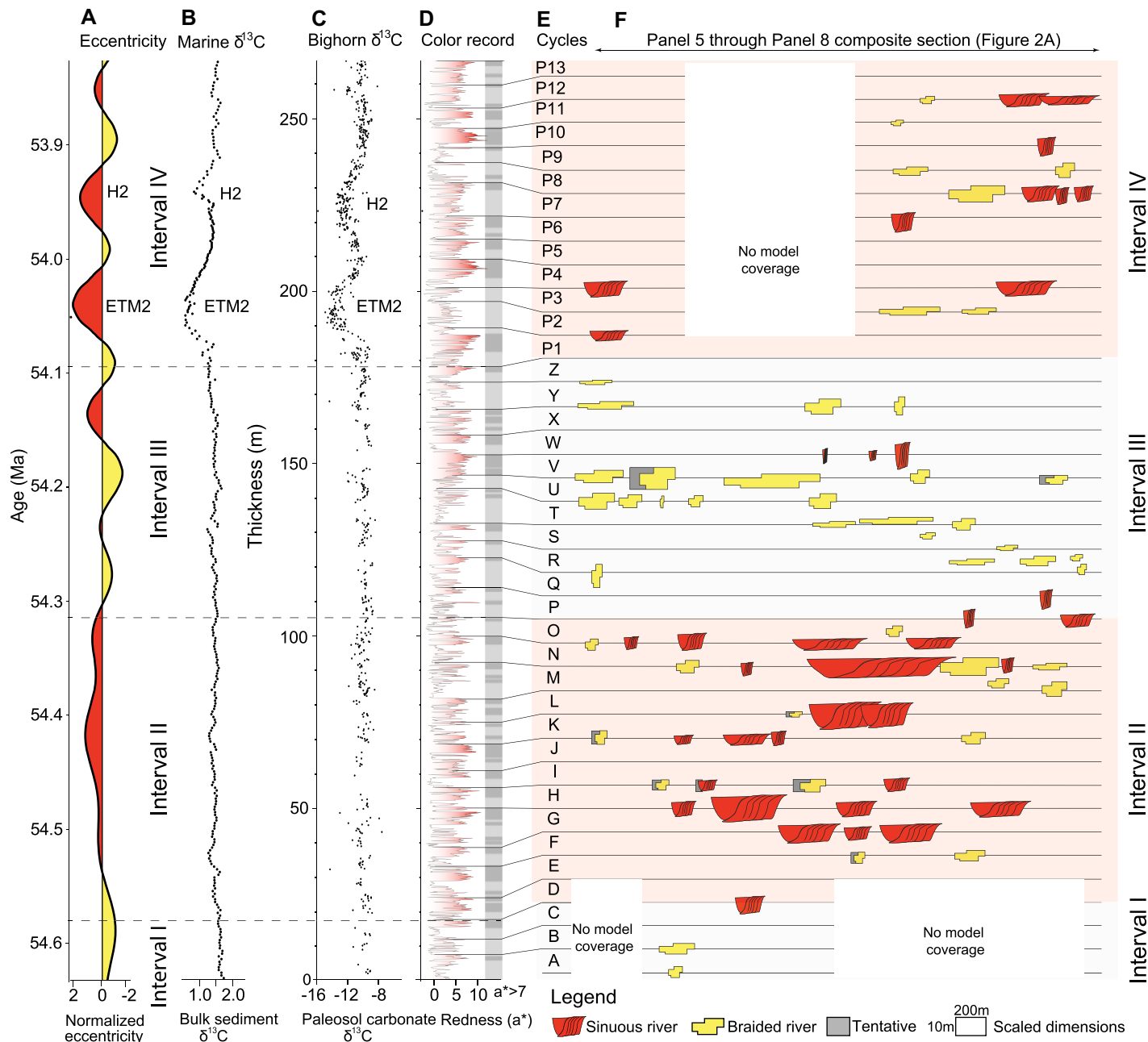
Figure 3. (A) Normalized eccentricity curve of Zeebe and Lourens (2019). ETM—Eocene Thermal Maximum; H2—hyperthermal event. **(B)** Stable carbon isotope stratigraphy from Ocean Drilling Program site 1262 (Walvis Ridge, southern Atlantic Ocean) of Zachos et al. (2010). **(C)** Stable carbon isotope stratigraphy from the Bighorn Basin (Wyoming, USA) of Abels et al. (2016). **(D)** Redness color reflectance record (data from Abels et al., 2013, 2016). **(E)** Notations for identified floodplain aggradation cycles from Wang et al. (2023). **(F)** Proportionally scaled sandstone bodies within the stratigraphic framework (see legend for scale).

by prolonged periods of oxidation, increased soil turnover, and sediment type conducive to enhanced drainage (Kraus and Aslan, 1993; Abels et al., 2013). Age control indicates overall constant sedimentation rates over the studied stratigraphy (Abels et al., 2016), and thus changing aggradation rates are not assumed to be the cause of changes in pedogenic intensity. Therefore, enhanced soil development may result from augmented channel stability that results in prolonged floodplain exposure to

pedogenesis, and from climatic conditions more suitable for paleosol development.

Mechanisms of Eccentricity Forcing of Alluvial Stratigraphy

In the Bighorn Basin, quasi-constant subsidence and substantial geographical separation from the paleo-shoreline have been reported (Foreman, 2014; Abels et al., 2016). Therefore, the observed alluvial stratigraphic change could result from climatic variations affecting both upstream areas and

the basin itself, which in turn influence water discharge, sediment flux, and vegetation cover (Vandenberghe, 2003; Kleinhans and van den Berg, 2011; Gibling and Davies, 2012). Walters et al. (2023) reported an increase in summer moisture and annual precipitation in southern Wyoming during periods termed OrbMaxN, which corresponds to periods of maximal eccentricity and obliquity and minimal precession. Their climate modeling suggests these trends are particularly valid for the Cordilleran uplift region, with simi-
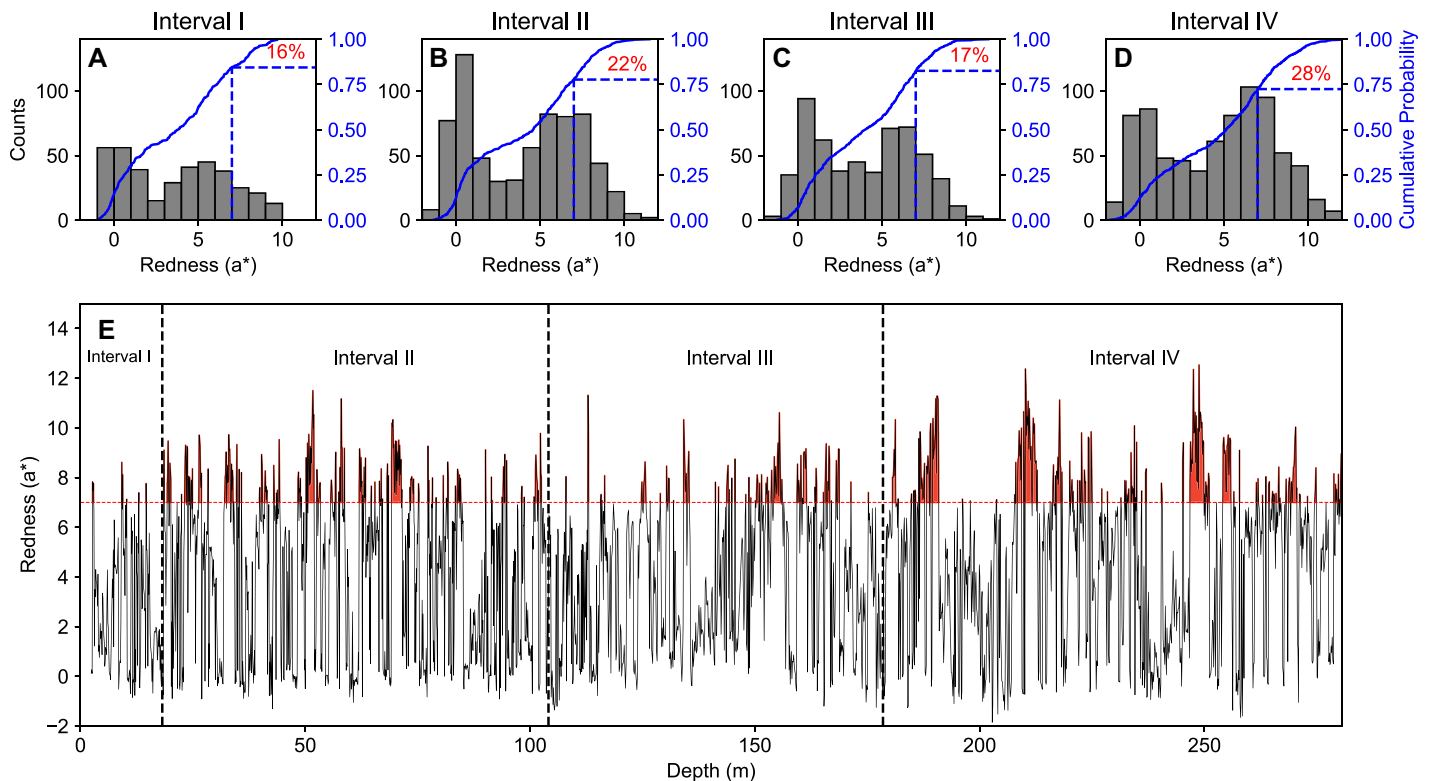
Figure 4. (A–D) Histograms and cumulative probability plots of redness in the Bighorn Basin, Wyoming, USA. Lower values indicate weaker pedogenesis, while higher values suggest substantial pedogenesis. Percentages represent the proportion of intense redness (a* > 7) within each interval. (E) Enlarged view of Figure 3D. Vertical dashed lines demarcate Intervals I–IV.

lar trends extending northward to the Bighorn Basin area. Consequently, eccentricity maxima in the Bighorn Basin are likely characterized by wetter conditions, and they are shown to produce predominant sinuous channels, more-developed paleosols, and lower sand content.

Building upon these past findings of climate modeling, we briefly explore the link between the long eccentricity-scale climatic variability and the observed stratigraphy, while acknowledging that this analysis is not exclusive. Specifically, the increased moisture levels during eccentricity maxima are posited to enhance vegetation density within both the catchment and basin. Such denser vegetation cover could diminish sediment transport and increase bank cohesion, thereby favoring sinuous channel formation and promoting paleosol development. Conversely, reduced vegetation during drier periods associated with eccentricity minima could lead to increased sediment fluxes and decreased bank stability, favoring braided channel formation and constraining paleosol development. This interpretation aligns with the eccentricity-driven landscape destabilization phases described by Smith et al. (2014). Our findings contribute to an improved understanding of how long-term climatic cycles may influence water discharge, sediment supply, and vegetation, thereby shaping alluvial stratigraphy. This improved understanding is vital for reconstructing past climate and predicting future landscape evolution.

REFERENCES CITED

Abels, H.A., Clyde, W.C., Gingerich, P.D., Hilgen, F.J., Fricke, H.C., Bowen, G.J., and Lourens, L.J., 2012, Terrestrial carbon isotope excursions and biotic change during Palaeogene hyperthermals: Nature Geoscience, v. 5, p. 326–329, https://doi.org/10.1038/ngeo1427.

Abels, H.A., Kraus, M.J., and Gingerich, P.D., 2013, Precession-scale cyclicity in the fluvial lower Eocene Willwood Formation of the Bighorn Basin, Wyoming (USA): Sedimentology, v. 60, p. 1467–1483, https://doi.org/10.1111/sed.12039.

Abels, H.A., Lauretano, V., van Yperen, A.E., Hopman, T., Zachos, J.C., Lourens, L.J., Gingerich, P.D., and Bowen, G.J., 2016, Environmental impact and magnitude of paleosol carbonate carbon isotope excursions marking five early Eocene hyperthermals in the Bighorn Basin, Wyoming: Climate of the Past, v. 12, p. 1151–1163, https://doi.org/10.5194/cp-12-1151-2016.

Blum, M.D., and Törnqvist, T.E., 2000, Fluvial responses to climate and sea-level change: A review and look forward: Sedimentology, v. 47, p. 2–48, https://doi.org/10.1046/j.1365-3091.2000.00008.x.

Church, M., 2006, Bed material transport and the morphology of alluvial river channels: Annual Review of Earth and Planetary Sciences, v. 34,

p. 325–354, https://doi.org/10.1146/annurev.earth.33.092203.122721.

Fielding, C.R., and Webb, J.A., 1996, Facies and cyclicity of the Late Permian Bainmedart Coal Measures in the Northern Prince Charles Mountains, MacRobertson Land, Antarctica: Sedimentology, v. 43, p. 295–322, https://doi.org/10.1046/j.1365-3091.1996.d01-6.x.

Fielding, C.R., Alexander, J., and Allen, J.P., 2018, The role of discharge variability in the formation and preservation of alluvial sediment bodies: Sedimentary Geology, v. 365, p. 1–20, https://doi.org/10.1016/j.sedgeo.2017.12.022.

Foreman, B.Z., 2014, Climate-driven generation of a fluvial sheet sand body at the Paleocene–Eocene boundary in north-west Wyoming (USA): Basin Research, v. 26, p. 225–241, https://doi.org/10.1111/bre.12027.

Foreman, B.Z., Heller, P.L., and Clementz, M.T., 2012, Fluvial response to abrupt global warming at the Palaeocene/Eocene boundary: Nature, v. 491, p. 92–95, https://doi.org/10.1038/nature11513.

Gibling, M., 2006, Width and thickness of fluvial channel bodies and valley fills in the geological record: A literature compilation and classification: Journal of Sedimentary Research, v. 76, p. 731–770, https://doi.org/10.2110/jsr.2006.060.

Gibling, M.R., and Davies, N.S., 2012, Palaeozoic landscapes shaped by plant evolution: Nature Geoscience, v. 5, p. 99–105, https://doi.org/10.1038/ngeo1376.

Hajek, E.A., and Straub, K.M., 2017, Autogenic sedimentation in clastic stratigraphy: Annual Review of Earth and Planetary Sciences, v. 45, p. 681–709, https://doi.org/10.1146/annurev-earth-063016-015935.

Huisink, M., 2000, Changing river styles in response to Weichselian climate changes in the Vecht valley, eastern Netherlands: Sedimentary Geology,

v. 133, p. 115–134, https://doi.org/10.1016/S0037-0738(00)00030-0.

Kleinhans, M., and van den Berg, J.H., 2011, River channel and bar patterns explained and predicted by an empirical and physics-based method: Earth Surface Processes and Landforms, v. 36, p. 721–738, https://doi.org/10.1002/esp.2090.

Kraus, M.J., and Aslan, A., 1993, Eocene hydromorphic paleosols: Significance for interpreting ancient floodplain processes: Journal of Sedimentary Research, v. 63, p. 453–463, https://doi.org/10.1306/D4267B22-2B26-11D7-8648000102C1865D.

Kraus, M.J., Woody, D., Smith, J.J., and Dukic, V., 2015, Alluvial response to the Paleocene–Eocene Thermal Maximum climatic event, Polecat Bench, Wyoming, USA: Palaeogeography, Palaeoclimatology, Palaeoecology, v. 435, p. 177–192, https://doi.org/10.1016/j.palaeo.2015.06.021.

Lyster, S.J., Whittaker, A.C., and Hajek, E.A., 2022, The problem of paleo-planforms: Geology, v. 50, p. 822–826, https://doi.org/10.1130/G49867.1.

Noorbergen, L., Turtu, A., Kuiper, K., Kasse, C., Ginneken, S., Dekkers, M., Krijgsman, W., Abels, H., and Hilgen, F., 2020, Long-eccentricity regulated climate control on fluvial incision and aggradation in the Palaeocene of north-eastern Montana (USA): Sedimentology, v. 67, p. 2529–2560, https://doi.org/10.1111/sed.12710.

Olsen, P.E., and Kent, D.V., 1996, Milankovitch climate forcing in the tropics of Pangaea during the Late Triassic: Palaeogeography, Palaeoclimatology, Palaeoecology, v. 122, p. 1–26, https://doi.org/10.1016/0031-0182(95)00171-9.

Opluštil, S., Laurin, J., Hýlová, L., Jirásek, J., Schmitz, M., and Sivek, M., 2022, Coal-bearing fluvial cycles of the late Paleozoic tropics; astronomical control on sediment supply constrained by high-precision radioisotopic ages, Upper Silesian Basin: Earth-Science Reviews, v. 228, 103998, https://doi.org/10.1016/j.earscirev.2022.103998.

Owen, A., Ebinghaus, A., Hartley, A.J., Santos, M.G.M., and Weissmann, G.S., 2017, Multi-scale classification of fluvial architecture: An exam-

ple from the Palaeocene–Eocene Bighorn Basin, Wyoming: Sedimentology, v. 64, p. 1572–1596, https://doi.org/10.1111/sed.12364.

Pujalte, V., Baceta, J.I., and Schmitz, B., 2015, A massive input of coarse-grained siliciclastics in the Pyrenean Basin during the PETM: The missing ingredient in a coeval abrupt change in hydrological regime: Climate of the Past, v. 11, p. 1653–1672, https://doi.org/10.5194/cp-11-1653-2015.

Sharma, N., Whittaker, A.C., Watkins, S.E., Valero, L., Vérité, J., Puigdefabregas, C., Adatte, T., Garcés, M., Guillocheau, F., and Castelltort, S., 2023, Water discharge variations control fluvial stratigraphic architecture in the Middle Eocene Escanilla formation, Spain: Scientific Reports, v. 13, 6834, https://doi.org/10.1038/s41598-023-33600-6.

Smith, M.E., Carroll, A.R., Scott, J.J., and Singer, B.S., 2014, Early Eocene carbon isotope excursions and landscape destabilization at eccentricity minima: Green River Formation of Wyoming: Earth and Planetary Science Letters, v. 403, p. 393–406, https://doi.org/10.1016/j.epsl.2014.06.024.

van Houten, F.B., 1944, Stratigraphy of the Willwood and Tatman formations in northwestern Wyoming: Geological Society of America Bulletin, v. 55, p. 165–210, https://doi.org/10.1130/GSAB-55-165.

Vandenberghe, J., 2001, A typology of Pleistocene cold-based rivers: Quaternary International, v. 79, p. 111–121, https://doi.org/10.1016/S1040-6182(00)00127-0.

Vandenberghe, J., 2003, Climate forcing of fluvial system development: An evolution of ideas: Quaternary Science Reviews, v. 22, p. 2053–2060, https://doi.org/10.1016/S0277-3791(03)00213-0.

Walters, A.P., Tierney, J.E., Zhu, J., Meyers, S.R., Graves, K., and Carroll, A.R., 2023, Climate system asymmetries drive eccentricity pacing of hydroclimate during the early Eocene greenhouse: Science Advances, v. 9, eadg8022, https://doi.org/10.1126/sciadv.adg8022.

Wang, Y., Storms, J.E.A., Martinius, A.W., Karssenberg, D., and Abels, H.A., 2021, Evaluating al-

luvial stratigraphic response to cyclic and non-cyclic upstream forcing through process-based alluvial architecture modelling: Basin Research, v. 33, p. 48–65, https://doi.org/10.1111/bre.12454.

Wang, Y., Baars, T.F., Sahoo, H., Storms, J.E.A., Martinius, A.W., Gingerich, P., and Abels, H.A., 2022, Sandstone body character and river planform styles of the lower Eocene Willwood Formation, Bighorn Basin, Wyoming, USA: Sedimentology, v. 69, p. 2897–2924, https://doi.org/10.1111/sed.13027.

Wang, Y., Baars, T.F., Storms, J.E.A., Martinius, A.W., Gingerich, P.D., Chmielewska, M., Buckley, S.J., and Abels, H.A., 2023, Lateral and vertical characteristics of floodplain aggradation cycles in the lower Eocene Willwood Formation, Bighorn Basin, Wyoming, USA: Geological Society of America Bulletin, https://doi.org/10.1130/B36908.1, (in press).

Ward, P.D., Montgomery, D.R., and Smith, R., 2000, Altered river morphology in South Africa related to the Permian-Triassic extinction: Science, v. 289, p. 1740–1743, https://doi.org/10.1126/science.289.5485.1740.

Westerhold, T., et al., 2020, An astronomically dated record of Earth's climate and its predictability over the last 66 million years: Science, v. 369, p. 1383–1387, https://doi.org/10.1126/science.aba6853.

Zachos, J.C., McCarren, H., Murphy, B., Röhl, U., and Westerhold, T., 2010, Tempo and scale of late Paleocene and early Eocene carbon isotope cycles: Implications for the origin of hyperthermals: Earth and Planetary Science Letters, v. 299, p. 242–249, https://doi.org/10.1016/j.epsl.2010.09.004.

Zeebe, R.E., and Lourens, L.J., 2019, Solar System chaos and the Paleocene–Eocene boundary age constrained by geology and astronomy: Science, v. 365, p. 926–929, https://doi.org/10.1126/science.aax0612.

Printed in the USA